Cell Systems

Report

Inferring Causal Gene Regulatory Networks from Coupled Single-Cell Expression Dynamics Using Scribe

Graphical Abstract

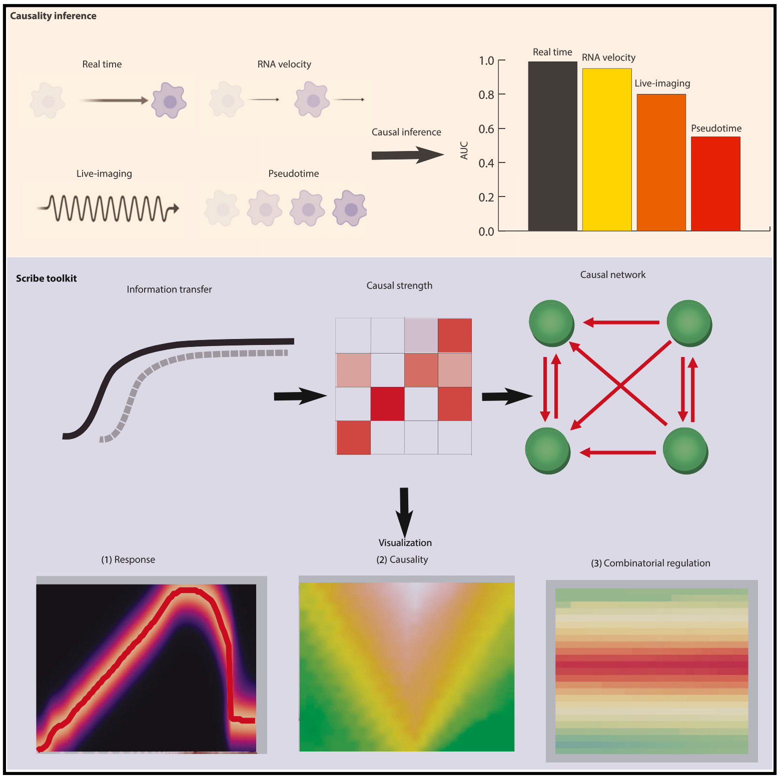

Highlights

- Scribe detects causal regulatory networks between genes in diverse single-cell datasets
- Scribe uses restricted directed information to identify regulators and their targets
- Inferring causal regulatory networks requires temporal coupling between measurements
- RNA velocity outperforms pseudotime, but neither perform as well as true time-series data

Authors

Xiaojie Qiu, Arman Rahimzamani,
Li Wang, ..., Lauren Saunders,
Cole Trapnell, Sreeram Kannan

Correspondence

coletrap@uw.edu (C.T.),
ksreeram@uw.edu (S.K.)

In Brief

Qiu et al. present Scribe (https://github.com/aristoteleo/Scribe-py), a toolkit for detecting and visualizing causal regulatory networks between genes in diverse single-cell datasets. They use Scribe to understand how causal network reconstruction depends on temporal coupling between measurements. They show that while pseudotime-ordered single-cell data fail to capture much of the information present in true temporal couplings, RNA velocity measurements restore much of this information.

Qiu et al., 2020, Cell Systems *10*, 1–10
March 25, 2020 © 2020 Elsevier Inc.
https://doi.org/10.1016/j.cels.2020.02.003

Please cite this article in press as: Qiu et al., Inferring Causal Gene Regulatory Networks from Coupled Single-Cell Expression Dynamics Using Scribe, Cell Systems (2020), https://doi.org/10.1016/j.cels.2020.02.003

Cell Systems
Report

Inferring Causal Gene Regulatory Networks from Coupled Single-Cell Expression Dynamics Using Scribe

Xiaojie Qiu,[1,2,8,9] Arman Rahimzamani,[3,8] Li Wang,[4] Bingcheng Ren,[5] Qi Mao,[6] Timothy Durham,[2] José L. McFaline-Figueroa,[2] Lauren Saunders,[1,2] Cole Trapnell,[1,2,7,10,*] and Sreeram Kannan[3,*]
[1]Molecular & Cellular Biology Program, University of Washington, Seattle, WA, USA
[2]Department of Genome Sciences, University of Washington, Seattle, WA, USA
[3]Department of Electrical Engineering, University of Washington, Seattle, WA, USA
[4]Department of Mathematics, University of Texas at Arlington, Arlington, TX, USA
[5]College of Information Science and Engineering, Hunan Normal University, Changsha, China
[6]HERE company, Chicago, IL 60606, USA
[7]Brotman-Baty Institute for Precision Medicine, Seattle, WA, USA
[8]These authors contributed equally
[9]Present address: Cellular Molecular Pharmacology, University of California, San Francisco, San Francisco, CA, USA
[10]Lead Contact
*Correspondence: coletrap@uw.edu (C.T.), ksreeram@uw.edu (S.K.)
https://doi.org/10.1016/j.cels.2020.02.003

SUMMARY

Here, we present Scribe (https://github.com/aristoteleo/Scribe-py), a toolkit for detecting and visualizing causal regulatory interactions between genes and explore the potential for single-cell experiments to power network reconstruction. Scribe employs restricted directed information to determine causality by estimating the strength of information transferred from a potential regulator to its downstream target. We apply Scribe and other leading approaches for causal network reconstruction to several types of single-cell measurements and show that there is a dramatic drop in performance for "pseudotime"-ordered single-cell data compared with true time-series data. We demonstrate that performing causal inference requires temporal coupling between measurements. We show that methods such as "RNA velocity" restore some degree of coupling through an analysis of chromaffin cell fate commitment. These analyses highlight a shortcoming in experimental and computational methods for analyzing gene regulation at single-cell resolution and suggest ways of overcoming it.

INTRODUCTION

Most biological processes, either in development or disease progression (Faith et al., 2007; Friedman et al., 2000; Langfelder and Horvath, 2008; Margolin et al., 2006; Meyer et al., 2008), are governed by complex gene regulatory networks. In the past few decades, numerous algorithms for inferring networks from observational gene expression data (Faith et al., 2007; Friedman et al., 2000; Langfelder and Horvath, 2008; Margolin et al., 2006; Meyer et al., 2008) have been developed.

Inferring a network of regulatory interactions between genes is challenging for two main reasons. The first challenge is that adding even a handful of genes to a network inference analysis requires that an algorithm consider many additional interactions between them (Figure 1A). Each of these potential regulatory interactions must be accepted or rejected on the basis of data. If a network that includes a particular gene regulatory interaction does not statistically "explain" the observed data substantially better than the network that excludes it, the interaction should be rejected. Deciding whether to include an interaction in a network is especially difficult because adding interactions risks overfitting to a particular dataset. Ultimately, as the number of edges explodes as the number of genes grows, so does the algorithms' demand for input data.

A second challenge in regulatory network inference is distinguishing upstream regulatory genes from their targets directly downstream. Most methods that aim to do so are predicated on the notion that changes in regulators should precede changes in their targets in time (Figure 1B) (Bar-Joseph et al., 2012). Granger causality (GC) (Granger, 1969) is a statistical hypothesis test for determining whether one time series (X_1) is useful in forecasting another (X_2), which has been applied to infer biological networks (Zou et al., 2009). However, GC assumes a linear relationship between the regulator and the target, which is violated in many biological settings (Hill et al., 2016). Convergent cross mapping (CCM) (Sugihara et al., 2012), a more recent technique based on state-space reconstruction (Takens, 1981) can detect pairwise non-linear interactions. However, this method is limited to deterministic systems, and thus may be poorly suited for many cellular processes (e.g., cell differentiation), which are inherently stochastic.

Single-cell RNA sequencing (scRNA-seq) experiments are attractive for gene regulatory network inference for two reasons. First, scRNA-seq experiments now routinely produce thousands

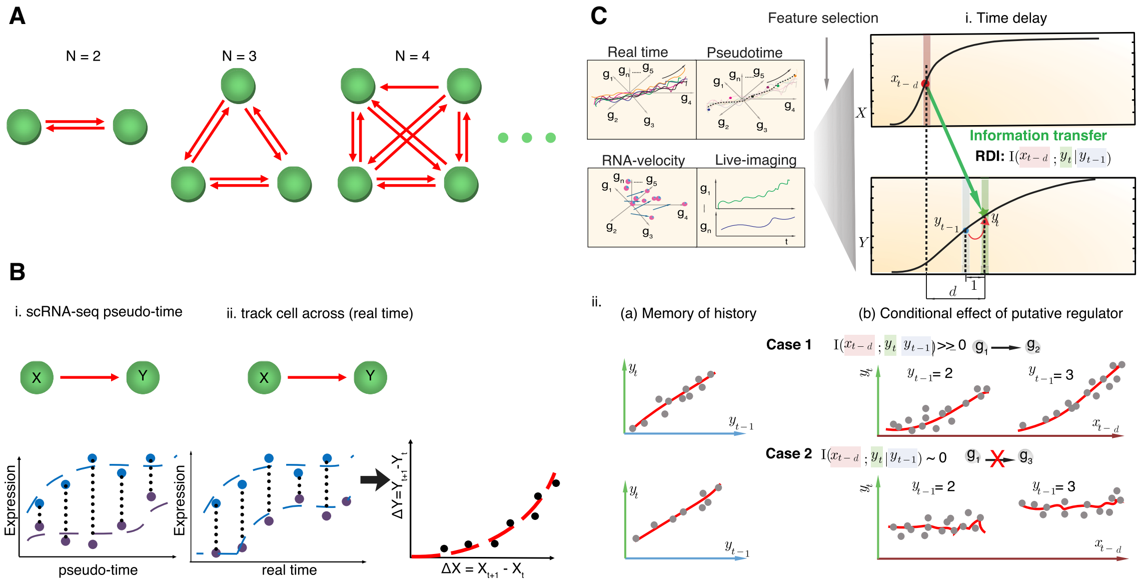

Figure 1. Scribe, a Toolkit for Inferring and Visualizing Causal Regulations

(A) Inferring regulatory networks from gene expression data is challenging because the number of regulatory interactions that must be evaluated grows much more quickly than the number of genes in the analysis.

(B) Ordering single-cell data in "pseudotime" or tracking how fluctuations in a regulatory network are followed by changes in a putative target in the same individual cells could boost power to detect causal regulatory interactions. Here, vertical dash lines indicate paired gene expression from the same cell, while horizontal dash lines indicates smoothed gene expression across cells from different pseudotime points (left) or across real time from the same cell (middle). The right panel represents the relationship of X/Y's gene expression difference between any two consecutive pseudotime or real-time points across cells or from the same cell.

(C) Scribe detects causality from four types of single-cell measurement ("pseudotime," "live image," "RNA velocity," and "real time") datasets with the metric, restricted directed information (RDI). Scribe relies on RDI (Rahimzamani and Kannan, 2016) to quantify the information transferred from the potential regulator to the target under some time delay while conditioned over its past on this pseudotime-series data. A gene often has a strong memory to its intermediate previous state (Y_{t-1}), but RDI will only give a highly positive causality score from the putative regulator to its target in cases where there is still a strong relationship between the regulator's history and the target's present condition on target's history (case 1 versus case 2).

of independent measurements, which may open the door to sufficiently powered inference (Liu and Trapnell, 2016). Second, algorithms that order the cells along "trajectories" that describe development or disease progress offer a tremendously high "pseudo-temporal" view of gene expression kinetics (Haghverdi et al., 2016; Qiu et al., 2017a; Setty et al., 2016; Trapnell et al., 2014). The recently introduced SCENIC method (Aibar et al., 2017) combines GENIE3 (Huynh-Thu et al., 2010) with regulatory binding motif enrichment to simultaneously cluster cells and infer regulatory networks. Other studies have inferred regulatory networks from scRNA-seq data using differential equations (Matsumoto et al., 2017; Ocone et al., 2015), information measures (Chan et al., 2017), Bayesian network analysis (Sanchez-Castillo et al., 2018), Boolean network methods (Hamey et al., 2017), or linear regression techniques (Huynh-Thu et al., 2010; Papili Gao et al., 2017; Wei et al., 2017). However, most methods do not explicitly leverage time-series data to identify causal interactions and more importantly, most fail to recover the correct network even in simple settings (Babtie et al., 2017; Fiers et al., 2018).

Here, we introduce Scribe, a scalable toolkit for inferring causal regulatory networks that relies on restricted directed information (RDI) (Rahimzamani and Kannan, 2016). In contrast to GC and CCM, Scribe learns both linear and non-linear causality in deterministic and stochastic systems. It also incorporates rigorous procedures to alleviate the sampling bias and builds upon improved estimators and regularization techniques to facilitate inference of large-scale causal networks. In concordance with the theory, we demonstrate that Scribe has superior performance compared to existing methods when the observations consist of true time-series data. However, current scRNA-seq protocols do not follow the same cells over time, breaking temporal coupling between measurements. We demonstrate that there is a dramatic drop in performance in causal network accuracy when the temporal coupling between measurements is lost. We then demonstrate that "RNA velocity," a recently developed analytic technique for scRNA-seq analysis, restores temporal coupling and improves causal regulatory network inference. Our results suggest that preserving this coupling should be a major objective of the next generation of single-cell measurement technologies.

RESULTS

Previously, we proposed RDI (Rahimzamani and Kannan, 2016, 2017), an information metric to accurately and efficiently quantify causality (STAR Methods). Here, we introduce Scribe, a toolkit built upon RDI, that is designed for the analysis of time-series datasets (either real time, RNA velocity, pseudotime or live imaging datasets), and is especially tailored for scRNA-seq (Figure S1;

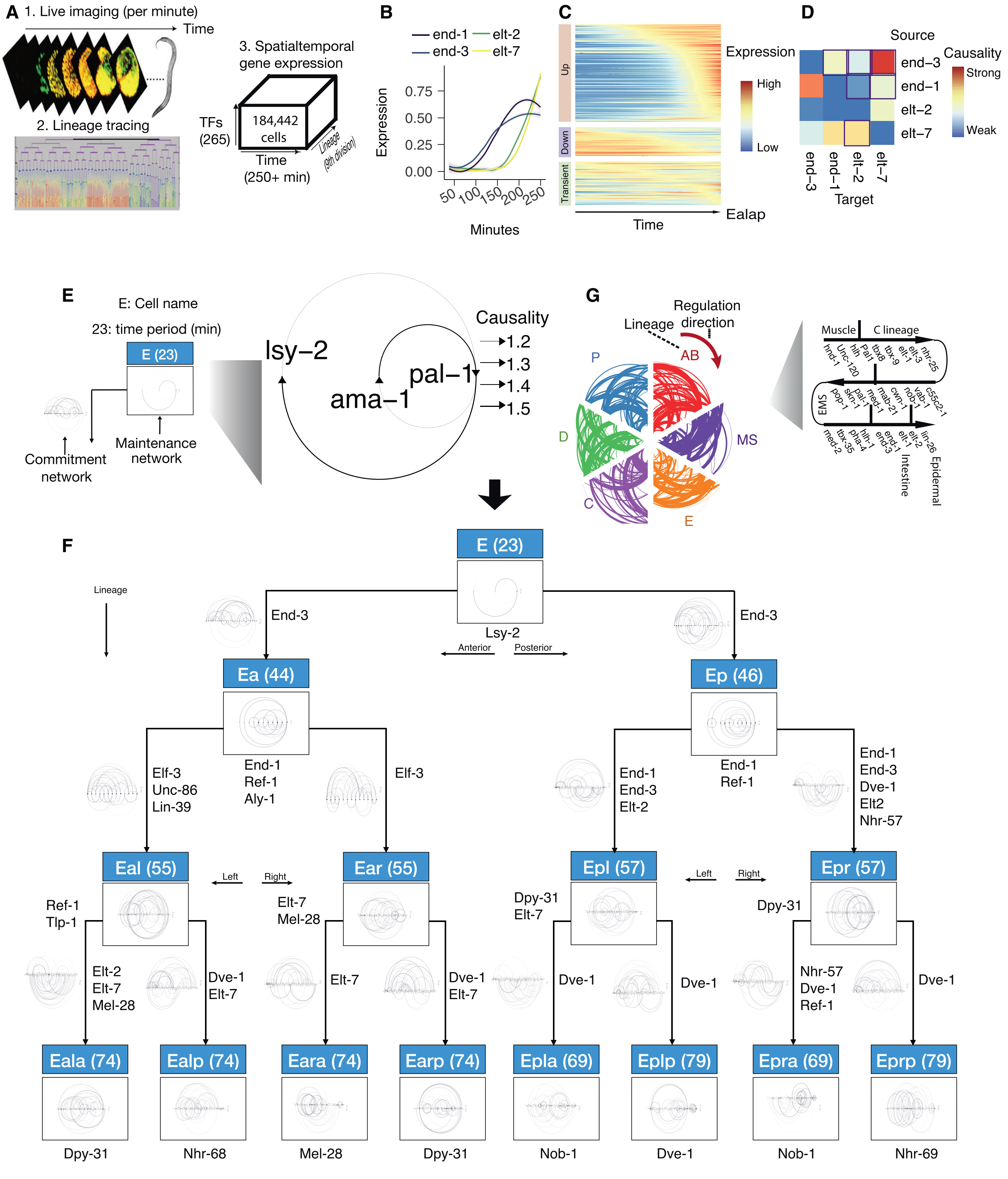

Figure 2. Live Imaging Dataset of *C. elegans* Early Embryogenesis Captures Transcription Expression Dynamics Hierarchy

(A) Scheme used by Murray et al. for measuring transcription factor's protein expression dynamics in real time for every cell during early *C. elegans* embryogenesis.

(B) Single-cell lineage-resolved fluorescence data capture temporal dynamics of *E* lineage master regulators during *C. elegans* embryogenesis. The expression for each gene is scaled to be between 0 and 1 and then smoothed using LOESS (locally estimated scatterplot smoothing) regression as in (Pliner et al., 2017), the same as in (C).

(legend continued on next page)

STAR Methods) and their visualization (Figure S2; STAR Methods).

In order to assess the performance of Scribe, we examined *Caenorhabditis elegans*' early embryogenesis, where live imaging has been used to measure nearly half of all transcription factors' (TFs') protein expression dynamics in every single cell in an embryo (Murray et al., 2012). This dataset consists of 265 time series each of which tracks the expression dynamics of a TF using fluorescent reporter constructs. Measurements were collected at 1-min intervals in every cell of the developing embryo for the first ~350 min of embryogenesis (Figure 2A).

We tested whether Scribe was able to learn validated genetic interactions that govern worm development. For example, it is understood that in the intestinal cell lineage *Ealap* the TFs end-1 and end-3 were upregulated prior to their targets elt-2 and elt-7 (Figure 2B and well before most other upregulated factors in this lineage (Figure 2C) (Wiesenfahrt et al., 2016). We ran Scribe on these four genes to determine whether it could correctly infer the causal regulatory interactions between them. Although Scribe captured some known causal interactions among the core TFs that specify this lineage (Owraghi et al., 2010), it also reported both false positive and false negative interactions based on previously curated networks (Owraghi et al., 2010; Wiesenfahrt et al., 2016). For example, Scribe reports that end-1 also strongly regulates end-3, which is not supported by previous studies (Owraghi et al., 2010; Wiesenfahrt et al., 2016) (Figure 2D). The entire *Ealap* lineage-specific network of *C. elegans* early embryogenesis constructed by Scribe is shown in Figures 2E–2G; zoomed-in versions of each network state is available in the Supplemental Information and Scribe's GitHub repository. Overall, Scribe was able to accurately infer known regulatory hierarchy (Figure 2F) (Murray et al., 2012).

Accurate Causal Network Inference Requires Temporally Coupled Expression Data

Next, we explored Scribe's ability to recover causal interactions using scRNA-seq, which in contrast to live imaging measures many genes in each cell. We first collected publicly available datasets from several biological systems including developing airway epithelium (Treutlein et al., 2014), dendritic cell response to antigen stimulation (Shalek et al., 2014), and myelopoiesis (Olsson et al., 2016). We then pseudo-temporally ordered these cells as previously described using Monocle 2 (Qiu et al., 2017a). Next, we ran Scribe on these pseudotime series (Figures 3 and S3) and examined the regulatory interactions reported for known transcriptional regulators of these systems. For each gene, we summed the causal interaction scores to all other genes, deriving a measure of its aggregate influence on the system. These aggregate causality scores were significantly higher for known transcriptional regulators than for genes believed to be targets by the authors of the original studies (unpaired two-sample t test, Figure S3).

We next explored whether Scribe can accurately reconstruct causal regulatory networks. Recently, Olsson and colleagues suggested a core network of TFs for regulating myelopoiesis (Olsson et al., 2016) by performing bulk ATAC-seq (assay for transposase-accessible chromatin using sequencing), chromatin immunoprecipitation sequencing (ChIP-seq), perturbation experiments, and profiling the transcriptomes of 382 cells from flow-sorted populations undergoing the transition (Figure 3A). We used Scribe to calculate causal scores for each regulator-target pair from the *Irf8* and *Gfi1* master regulators of the monocyte or granulocyte lineage as identified by Olsson et al., respectively, to the other six genes in the core network, using scRNA-seq data alone. We hypothesized that Scribe would return strong causal scores for the targets ascribed to each regulator but not others. We observed that expression kinetics over pseudotime correctly reflect the network architecture (Figures 3A and 3B). We represent the causal network inferred by Scribe as a heatmap where each row corresponds to the causal score from the regulator to all other genes and the color corresponds to the magnitude of the causal score (Figure 3C). Scribe assigns a high causality score for all targets of *Irf8* (*Gfi1*, *Irf5*, *Klf4*, *Per3*, and *Zeb2*) but lowest causality score to *Irf8* and *Ets1*, which are not its direct targets. Similarly, Scribe assigns a high causality score for the majority of Gfi1's targets (*Irf8*, *Klf4*, and *Per3*) even though *Gfi1* has low expression values (Figure 3C). Visualization of the combinatorial regulation of *Irf8* and *Gfi1* to either *Zeb2* or *Per3*, based on the Scribe visualization toolkit, captures the conflicting regulation pattern between two regulators and their two targets (Figure 3D).

To determine Scribe's capabilities to reconstruct transcriptome-level causal networks containing edges between TFs as well as from TFs to putative downstream targets, we applied Scribe to scRNA-seq data of hematopoiesis (Paul et al., 2015). We find that the lineage-specific genes tend to have a high total outgoing RDI sum among all significant TFs (Figure 3E). When restricting to a small subset of previously identified erythropoiesis-associated TFs, we find Scribe identified several regulatory interactions, such as *Gata1-Gfi1-Klf4*, which are known to play an important role in myelopoiesis (Laslo et al., 2006; Stopka et al., 2005; Tamura et al., 2015) (Figure 3F). However, in recovering known regulatory interactions in each system based on a manually curated network from the literature, Scribe only marginally outperformed GC and CCM but all three methods generally performed poorly, with no method reaching an area under curve (AUC) of greater than 0.7 (Figures 3G–3I).

We hypothesized that as with live imaging datasets, a lack of coupling between the expression measurements in pseudo-temporally ordered scRNA-seq data leads to poor accuracy during regulatory network inference. In contrast to a true time series in which an individual cell is tracked and measured longitudinally, in pseudo-temporal datasets, each expression measurement comes from a different cell. Therefore, although pseudotime

(C) Expression dynamics for 265 reported TFs along the lineage leading to the *Ealap* cell.

(D) Scribe reconstructs the causal regulatory network for the four master regulators (*end-1/3* and *elt-2/7*). Note that the outlined box corresponds to the previously known regulations.

(E) A scheme for the multiscale network for (F).

(F) An integrative multiscale model for the (E) lineage specification. Zoom in to see the network architecture in details.

(G) Lineage (AB, P, MS, E, D, C; Sulston et al., 1983) -specific causal networks for the curated master regulators constructed with Scribe shown as a hive plot.

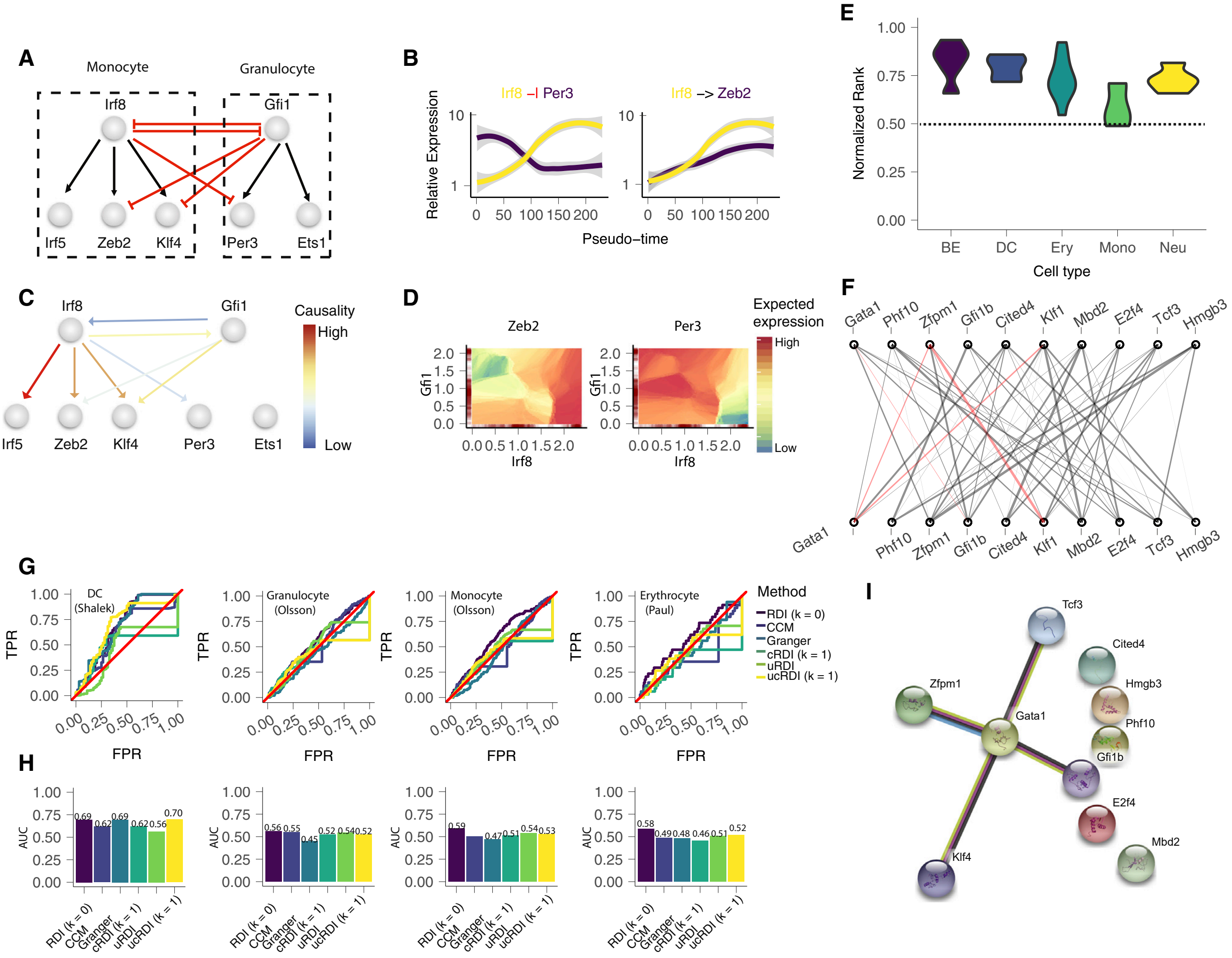

Figure 3. Scribe Recovers a Core Regulatory Network Responsible for Myelopoiesis

(A) A core network describes key regulators during the specification of monocytes and granulocytes (Olsson et al., 2016).

(B) Examples of gene-target pair kinetic curves over pseudotime along the monocyte lineage.

(C) Scribe infers the expected core regulatory network interactions for myelopoiesis.

(D) Visualization of combinatorial gene regulation from *Irf8* and *Gfi1* to *Zeb2* or *Per3*.

(E) The normalized rank of lineage-specific genes' total outgoing RDI sum.

(F) Lineage-specific network of significant regulators during erythropoiesis. Edges supported by the spring database are colored as red lines. For (E) and (F), BEAM analysis was used to identify significant branching genes associated with the four (one) lineage bifurcation events shown in the hematopoietic trajectory from Qiu et al. (2017a) based on the Paul dataset (Paul et al., 2015). The top 1,000 differentially expressed genes associated with each bifurcation were chosen to build a causal network for each relevant lineage. A set of TFs relevant to specific lineages described previously is used for (E) or (F). Neu, neutrophil; Ery, erythroid; Mk, megakaryocyte; mono, monocyte; DC, dendritic cell; BE, basophil and eosinophil.

(G and H) Receiver operating curves (ROC) (G, top) and area under curve (AUC) (H, bottom) of the inferred causal network based on Scribe, GC, and CCM, from left to right, on the dendritic cell (DC) dataset, granulocyte or monocyte branch of the Olsson dataset, and erythroid branch of the Paul dataset. Four different variants of causal inference implemented in Scribe are tested: *RDI (L =0)*, the default RDI method without conditioning on any other gene; *RDI (L = 1)*, the RDI method based on conditioning on the incoming gene with highest causality score, except the current target; *uRDI*, the method based on the uniformization technique applied on the actual distribution in RDI; and *uRDI (L = 1)*, the uRDI method but also with the conditioning on the incoming gene with the highest causality score, except the current target.

(I) The network of the gene set as included in (F) retrieved from the STRING database.

reveals overall trends of the gene expression dynamics, the real-time gene expression "micro-fluctuations" (fluctuations that happen within short time-scales) of a regulator to a target is not captured in pseudotime.

To test whether causal network inference requires temporal coupling between genes across measurements, we ran Scribe on simulated data based on a core network of neurogenesis (STAR Methods) collected using four strategies for obtaining longitudinal measurements from individual cells. First, we consider "real time," an ideal theoretical technology in which all genes are tracked in each individual cell as that cell differentiates. We therefore consider a second setting "live imaging," in which

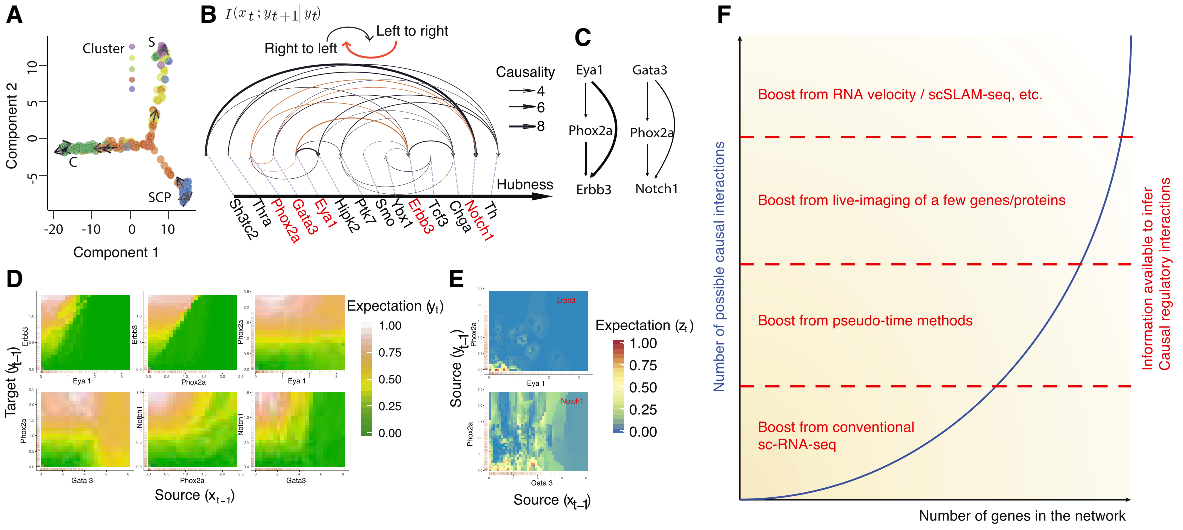

Figure 4. Causal Inference in Scribe with RNA Velocity

(A) RNA velocity vector projected onto the first two latent dimensions. A small subset of arrows is used to visualize the velocity field of the cells. S, sympathoblasts; C, chromaffin; SCP, Schwann cell progenitor. The color of each cell corresponds to the cluster id from Figure 5B of (Furlan et al., 2017).

(B) A core causal network for chromaffin cell commitment inferred based on RNA velocity. Gene set is collected from (Furlan et al., 2017). Context likelihood of relatedness (CLR) regularization is used to remove spurious causal edges in the network (see STAR Methods).

(C) Two potential coherent feed-forward loop (FFL) motifs of chromaffin differentiation are discovered from the core network. Edge width corresponds to causal regulation strength.

(D) Visualization of the six causal regulation pairs in the feed-forward loops of *Eya1-Phox2a-Erbb3* and *Gata3-Phox2a-Notch1* (see STAR Methods for details).

(E) Visualizing combinatorial regulation logic for the two feed-forward loops in (C) with Scribe. For both (D) and (E), a grid with 625 cells (25 on each dimension) is used. Similarly, expected values are scaled by the maximum to obtain a range from 0 to 1.

(F) Scribe's ability to detect causal regulatory interactions is limited by the single-cell measurement technology used. Technologies that provide measurements that are coupled across time and between genes provide more power for inference than conventional single-cell RNA-seq experiments.

each cell is tracked over time but only one gene is measured. Third, we examine pseudotime, where all genes are measured only once in distinct cells that have been sampled from a population undergoing differentiation. Finally, we tested Scribe on RNA velocity data, which consists of a snapshot measurement of each cell's current transcriptome along with a prediction of that same cell's expression levels at a short time in the future (Figure S4A).

Using pseudo-temporal measurements, GC, CCM, and Scribe all performed very poorly in recovering direct, causal interactions between genes in the hypothetical network (Figure S4B). The inability of these methods to recover regulatory interactions is unlikely to be due to the undersampling of the system, as the performance was insensitive to varying the number of cells captured in the simulated datasets (Figures S4C and S4D). Performance of the three methods was only modestly better when using data captured by "live imaging."

We next evaluated two alternative modes of measuring gene expression dynamics in single cells in which fluctuations are coupled. Using conditional RDI, Scribe produced highly accurate reconstructions from "real-time" measurements of gene expression (AUC: 0.859 ± 0.0283), in which every gene is measured repeatedly in a set of cells as they differentiate. This demonstrates that when measurements are fully coupled across time, and fluctuations in a regulator can propagate to its targets, restricted directed information correctly reveals causal regulatory interactions. Scribe also recovered accurate networks (AUC: 0.837 ± 0.0189) with "RNA velocity" measurements (Figure S4A). Although RNA velocity does not repeatedly measure cells, it provides a "prediction" of the future expression levels of each gene based on comparing mature to immature transcript levels, in effect introducing a form of temporal coupling to the data. These simulations show that methods for regulatory inference based on information transfer fail using data from measurement modalities in which fluctuation of a regulator's expression across cells is "uncoupled" from fluctuations in its targets.

Causal Network Inference with "RNA Velocity" Reveals Regulatory Interactions that Drive Chromaffin Cell Differentiation

We next sought to test whether Scribe could recover causal network interactions using real RNA velocity measurements. Recently, La Manno and colleagues applied RNA velocity to study chromaffin cell differentiation as well as their associated cell cycle dynamics (La Manno et al., 2018). We used this chromaffin dataset as a proof of principle for incorporating "RNA velocity" into Scribe. We first reconstructed a developmental trajectory from mature mRNA expression levels from each cell in this dataset and then applied branch expression analysis odeling, or BEAM (Qiu et al., 2017b), to identify genes that significantly bifurcate between Schwann and chromaffin cell branches (Figure 4). These genes were enriched in processes related to neuron differentiation along the path from Schwann cell progenitors (SCPs) to mature chromaffin cells (Figure S4E).

We then applied Scribe to the RNA velocity measurements from the 3,665 significantly branch-dependent genes (q value < 0.01, Benjamini-Hochberg correction) (Figures 4C and S4). We first built a network between significant branching TFs as well as from TFs to the significant targets in chromaffin lineage and found that only 0.75% of TFs interact with each other while 8.40% of TFs regulate potential targets (causality score > 0.05) (Figures 4E–4G). We then inferred a core network between fourteen TFs believed to drive chromaffin cell differentiation (Furlan et al., 2017). Within this core network, Scribe identified two feed-forward loop (FFL) motifs (Alon, 2007): *Eya1-Phox2a-Erbb3* and *Gata3-Phox2a-Notch1* (Figures 4C–4E). The STRING (Search Tool for the Retrieval of Interacting Genes/Proteins) database of genetic and molecular interactions (Szklarczyk et al., 2017) provided additional support for these regulatory motifs (Figure S4H). From the RNA velocity network, we also find that SCP-related TFs, such as *Sh3tc2*, tend to have stronger causal regulation (ranked higher in terms of hubness as shown in the arc plot), while chromaffin cell-related TFs, including *Chga* and *Th*, have much smaller causal regulations, reflecting the network capture transition from SCPs to chromaffin cells (Furlan et al., 2017).

DISCUSSION

Despite extensive research into gene regulatory network inference over the past several decades, the fundamental source of poor performance by these methods on single-cell data remains uncertain. One possibility is that, even with the tremendous gains in the throughput achieved by the developers of scRNA-seq technology over the past decade (Svensson and Vento-Tormo, 2017), these methods still have not been provided with sufficient data to accurately reconstruct networks. Alternatively, the basic approach of inferring genetic interactions based on statistical interactions between their measured expression levels may be fundamentally limited.

We developed Scribe, which uses recently reported advances in information theory to infer complex causal regulatory interactions between genes. Scribe employs RDI, overcoming limitations inherent to GC and CCM. Scribe also provides several ways to visualize causal information transfer, helping users distinguish between direct and indirect interactions and unravel combinatorial regulatory logic.

Although Scribe correctly infers causal regulatory interactions in simulated measurements that track all the genes in an individual cell over time, it performs poorly on live imaging or pseudotemporally ordered single-cell datasets. We demonstrate that poor performance is due to the loss of temporal coupling between measurements of genes that interact, in which fluctuations in the levels of a regulator propagate to measurements of its targets. This may explain poor performance by a broad class of information-theoretic or statistical approaches for inferring regulatory networks from scRNA-seq data. If so, then simply improving the throughput of scRNA-seq protocols will not be sufficient to power inference methods. Pseudo-temporally ordering scRNA-seq data provides a boost to the number of genes that may be considered, and the temporal coupling provided from joint measurement via live imaging of pairs of genes could boost power further (Figure 4F).

Improvements to single-cell expression assays that produce measurements for multiple genes that are coupled across time may enable the accurate regulatory network inference possible using Scribe or similar approaches. Although methods for nondestructively tracking expression levels of many genes in single cells over time have not been described, several assays have been reported that provide snapshot estimates of both steady-state mRNA levels along with their rates of synthesis. These assays report measurements of the current and future transcriptome of individual cells, essentially providing temporal coupling over a short time horizon. For example, SLAM-seq (thiol(SH)-linked alkylation for the metabolic sequencing of RNA) (Herzog et al., 2017; Muhar et al., 2018) or TUC-seq (thiouridine-to-cytidine sequencing) (Riml et al., 2017) assay mature RNA levels and estimate the rate of their synthesis via nucleotide-labeling or conversion-based approaches. Importantly, single-cell versions of those technologies (Cao et al., 2019; Erhard et al., 2019; Hendriks et al., 2018; Qiu et al., 2019) have recently been developed when this paper was under review and awaits integrating Scribe with those technologies as future investigation. Sequential, multiplex RNA fluorescence *in situ* hybridization (FISH) or ‘‘Seq-FISH’’ (Shah et al., 2018) which probes both exons and introns of RNAs can also provide similar measurements. RNA velocity, which analyzes scRNA-seq reads falling within introns and estimates both mature mRNA levels and their immature intermediates to predict the transcriptome over a short time in the future, also generates coupled measurements. Accordingly, using RNA velocity measurements greatly improves Scribe's accuracy compared to running it on pseudotemporal scRNA-seq measurements. These assays and algorithmic improvements boost Scribe's ability to recover causal interactions because they provide increasingly comprehensive and temporally coupled measurements across the transcriptome. Concentrating efforts to improve temporal coupling in new experimental methods should, in our view, be a priority for the field.

scRNA-seq holds great promise for powering various algorithms for network inference but as we have shown, major obstacles remain in the way of doing so in practice. Once provided with temporally coupled measurements, Scribe accurately reconstructs networks of modest scale. As experimental and computational improvements to single-cell expression techniques couple measurements across time, we expect Scribe to be increasingly capable of dissecting the complex genetic circuits that drive development and disease.

STAR★METHODS

Detailed methods are provided in the online version of this paper and include the following:

- KEY RESOURCES TABLE
- LEAD CONTACT AND MATERIALS AVAILABILITY
- METHOD DETAILS
  - ○ Four Possible Single-Cell Time-Series Measurement Modalities
  - ○ The Problem of Causal Regulatory Network Inference
  - ○ Causal Inference
  - ○ Granger Causality
  - ○ Kernel Granger Causality
  - ○ Convergent Cross Mapping

  - Restricted Directed Information (RDI)
  - Uniformization Method for Adjusting Sampling Bias
  - Scribe: A Toolkit for Visualization and Detection of Complex Causal Regulation from Single-Cell Genomics Datasets
  - Preparing Pseudotime-Series or RNA-Velocity for scRNA-seq Datasets
  - Visualizing Pairwise Gene Interaction
  - Visualizing Combinatorial Gene Regulation
  - Causal Network Inference: an RDI-Based Algorithm
  - Inferring and Visualizing Transcriptomic Gene Regulatory Network
  - Parameters of RDI
  - Algorithm Complexity
  - Regularizing Causal Interaction Networks
  - Benchmarking Scribe with Alternative Algorithms on Inferring Causal Regulatory Network
  - Ordinary Differential Equations for the Neuron System
  - Details on Analyzing Datasets Used in This Study
- DATA AND CODE AVAILABILITY
  - Code Availability
  - Data Availability

SUPPLEMENTAL INFORMATION

Supplemental Information can be found online at https://doi.org/10.1016/j.cels.2020.02.003.

ACKNOWLEDGMENTS

We thank Robert Waterston and his lab for guidance in analyzing *C. elegans* early embryogenesis, Gioele La Manno for discussing causal network inference with RNA velocity, Andysheh Mohajeri for helping to prepare a website for this work, and members of the Trapnell laboratory for comments on the manuscript. This work was supported by a US National Institutes of Health (NIH) grant DP2 HD088158, the Paul G. Allen Frontiers Group (Allen Discovery Center grant to C.T.), and the W.M. Keck Foundation (to C.T.). C.T. is partly supported by an Alfred P. Sloan Foundation Research Fellowship. A.R. and S.K. were funded in part by an NIH award 1R01HG008164, an NSF Career award 1651236, and an NSF CCF award 1703403.

AUTHOR CONTRIBUTIONS

X.Q., A.R., C.T., and S.K. designed Scribe. X.Q. and A.R. implemented the methods. X.Q. and A.R. performed the analysis. L.W., B.R., Q.M., T.D., J.L.M.-F., and L.S. contributed to the data analysis. X.Q., C.T., and S.K. conceived the project. All authors wrote the manuscript.

DECLARATION OF INTERESTS

The authors declare no competing interests.

Received: September 12, 2018
Revised: June 8, 2019
Accepted: February 5, 2020
Published: March 4, 2020

REFERENCES

Aibar, S., González-Blas, C.B., Moerman, T., Huynh-Thu, V.A., Imrichova, H., Hulselmans, G., Rambow, F., Marine, J.C., Geurts, P., Aerts, J., et al. (2017). SCENIC: single-cell regulatory network inference and clustering. Nat. Methods *14*, 1083–1086.

Alon, U. (2007). Network motifs: theory and experimental approaches. Nat. Rev. Genet. *8*, 450–461.

Amit, I., Garber, M., Chevrier, N., Leite, A.P., Donner, Y., Eisenhaure, T., Guttman, M., Grenier, J.K., Li, W., Zuk, O., et al. (2009). Unbiased reconstruction of a mammalian transcriptional network mediating pathogen responses. Science *326*, 257–263.

Babtie, A.C., Chan, T.E., and Stumpf, M.P.H. (2017). Learning regulatory models for cell development from single cell transcriptomic data. Curr. Opin. Syst. Biol. *5*, 72–81.

Bar-Joseph, Z., Gitter, A., and Simon, I. (2012). Studying and modelling dynamic biological processes using time-series gene expression data. Nat. Rev. Genet. *13*, 552–564.

Cao, J., Zhou, W., Steemers, F., Trapnell, C., and Shendure, J. (2019). Characterizing the temporal dynamics of gene expression in single cells with sci-fate. bioRxiv. https://doi.org/10.1101/666081.

Chan, T.E., Stumpf, M.P.H., and Babtie, A.C. (2017). Gene regulatory network inference from single-cell data using multivariate information measures. Cell Syst. *5*, 251–267.e3.

Cover, T.A., and Thomas, J.A. (2006). Elements of information theory (John Wiley & Sons).

Erhard, F., Baptista, M.A.P., Krammer, T., Hennig, T., Lange, M., Arampatzi, P., Jürges, C.S., Theis, F.J., Saliba, A.E., and Dölken, L. (2019). scSLAM-seq reveals core features of transcription dynamics in single cells. Nature *571*, 419–423.

Faith, J.J., Hayete, B., Thaden, J.T., Mogno, I., Wierzbowski, J., Cottarel, G., Kasif, S., Collins, J.J., and Gardner, T.S. (2007). Large-scale mapping and validation of Escherichia coli transcriptional regulation from a compendium of expression profiles. PLoS Biol. *5*, e8.

Fiers, M.W.E.J., Minnoye, L., Aibar, S., Bravo González-Blas, C., Kalender Atak, Z., and Aerts, S. (2018). Mapping gene regulatory networks from single-cell omics data. Brief. Funct. Genomics *17*, 246–254.

Friedman, N., Linial, M., Nachman, I., and Pe'er, D. (2000). Using Bayesian networks to analyze expression data. J. Comput. Biol. *7*, 601–620.

Furlan, A., Dyachuk, V., Kastriti, M.E., Calvo-Enrique, L., Abdo, H., Hadjab, S., Chontorotzea, T., Akkuratova, N., Usoskin, D., Kamenev, D., et al. (2017). Multipotent peripheral glial cells generate neuroendocrine cells of the adrenal medulla. Science *357*, eaal3753.

Garber, M., Yosef, N., Goren, A., Raychowdhury, R., Thielke, A., Guttman, M., Robinson, J., Minie, B., Chevrier, N., Itzhaki, Z., et al. (2012). A high-throughput chromatin immunoprecipitation approach reveals principles of dynamic gene regulation in mammals. Mol. Cell *47*, 810–822.

Granger, C.W.J. (1969). Investigating causal relations by econometric models and cross-spectral methods. Econometrica *37*, 424.

Haghverdi, L., Büttner, M., Wolf, F.A., Buettner, F., and Theis, F.J. (2016). Diffusion pseudotime robustly reconstructs lineage branching. Nat. Methods *13*, 845–848.

Hamey, F.K., Nestorowa, S., Kinston, S.J., Kent, D.G., Wilson, N.K., and Göttgens, B. (2017). Reconstructing blood stem cell regulatory network models from single-cell molecular profiles. Proc. Natl. Acad. Sci. USA *114*, 5822–5829.

Hendriks, G.-J., Jung, L.A., Larsson, A.J.M., Forsman, O.A., Lidschreiber, M., Lidschreiber, K., Cramer, P., and Sandberg, R. (2018). NASC-seq monitors RNA synthesis in single cells. Nat. Commun. *10*, 3138.

Herzog, V.A., Reichholf, B., Neumann, T., Rescheneder, P., Bhat, P., Burkard, T.R., Wlotzka, W., von Haeseler, A., Zuber, J., and Ameres, S.L. (2017). Thiol-linked alkylation of RNA to assess expression dynamics. Nat. Methods *14*, 1198–1204.

Hill, S.M., Heiser, L.M., Cokelaer, T., Unger, M., Nesser, N.K., Carlin, D.E., Zhang, Y., Sokolov, A., Paull, E.O., Wong, C.K., et al. (2016). Inferring causal molecular networks: empirical assessment through a community-based effort. Nat. Methods *13*, 310–318.

Huynh-Thu, V.A., Irrthum, A., Wehenkel, L., and Geurts, P. (2010). Inferring regulatory networks from expression data using tree-based methods. PLoS One *5*.

Kleinberg, J.M. (1999). Authoritative sources in a hyperlinked environment. J. ACM *46*, 604–632.

Kraskov, A., Stögbauer, H., and Grassberger, P. (2004). Estimating mutual information. Phys Rev E Stat Nonlin Soft Matter Phys *69*, 066138.

Krishnaswamy, S., Spitzer, M.H., Mingueneau, M., Bendall, S.C., Litvin, O., Stone, E., Pe'er, D., and Nolan, G.P. (2014). Systems biology. Conditional density-based analysis of T cell signaling in single-cell data. Science *346*, 1250689.

La Manno, G., Soldatov, R., Zeisel, A., Braun, E., Hochgerner, H., Petukhov, V., Lidschreiber, K., Kastriti, M.E., Lönnerberg, P., Furlan, A., et al. (2018). RNA velocity of single cells. Nature *560*, 494–498.

Langfelder, P., and Horvath, S. (2008). WGCNA: an R package for weighted correlation network analysis. BMC Bioinformatics *9*, 559.

Laslo, P., Spooner, C.J., Warmflash, A., Lancki, D.W., Lee, H.J., Sciammas, R., Gantner, B.N., Dinner, A.R., and Singh, H. (2006). Multilineage transcriptional priming and determination of alternate hematopoietic cell fates. Cell *126*, 755–766.

Liu, S., and Trapnell, C. (2016). Single-cell transcriptome sequencing: recent advances and remaining challenges. F1000Res *5*, https://doi.org/10.12688/f1000research.7223.1.

Ma, W., Trusina, A., El-Samad, H., Lim, W.A., and Tang, C. (2009). Defining network topologies that can achieve biochemical adaptation. Cell *138*, 760–773.

Margolin, A.A., Nemenman, I., Basso, K., Wiggins, C., Stolovitzky, G., Dalla Favera, R., and Califano, A. (2006). ARACNE: an algorithm for the reconstruction of gene regulatory networks in a mammalian cellular context. BMC Bioinformatics *7*, S7.

Marinazzo, D., Pellicoro, M., and Stramaglia, S. (2008). Kernel method for nonlinear granger causality. Phys. Rev. Lett. *100*, 144103.

Matsumoto, H., Kiryu, H., Furusawa, C., Ko, M.S.H., Ko, S.B.H., Gouda, N., Hayashi, T., and Nikaido, I. (2017). SCODE: an efficient regulatory network inference algorithm from single-cell RNA-Seq during differentiation. Bioinformatics *33*, 2314–2321.

Meyer, P.E., Lafitte, F., and Bontempi, G. (2008). minet: A R/bioconductor package for inferring large transcriptional networks using mutual information. BMC Bioinformatics *9*, 461.

Muhar, M., Ebert, A., Neumann, T., Umkehrer, C., Jude, J., Wieshofer, C., Rescheneder, P., Lipp, J.J., Herzog, V.A., Reichholf, B., et al. (2018). SLAM-seq defines direct gene-regulatory functions of the BRD4-MYC axis. Science *360*, 800–805.

Murray, J.I., Boyle, T.J., Preston, E., Vafeados, D., Mericle, B., Weisdepp, P., Zhao, Z., Bao, Z., Boeck, M., and Waterston, R.H. (2012). Multidimensional regulation of gene expression in the C. elegans embryo. Genome Res. *22*, 1282–1294.

Ocone, A., Haghverdi, L., Mueller, N.S., and Theis, F.J. (2015). Reconstructing gene regulatory dynamics from high-dimensional single-cell snapshot data. Bioinformatics *31*, i89–i96.

Olsson, A., Venkatasubramanian, M., Chaudhri, V.K., Aronow, B.J., Salomonis, N., Singh, H., and Grimes, H.L. (2016). Single-cell analysis of mixed-lineage states leading to a binary cell fate choice. Nature *537*, 698–702.

Owraghi, M., Broitman-Maduro, G., Luu, T., Roberson, H., and Maduro, M.F. (2010). Roles of the Wnt effector POP-1/TCF in the C. elegans endomesoderm specification gene network. Dev. Biol. *340*, 209–221.

Papili Gao, N., Ud-Dean, S.M.M., Gandrillon, O., and Gunawan, R. (2017). SINCERITIES: inferring gene regulatory networks from time-stamped single cell transcriptional expression profiles. Bioinformatics *34*, 258–266.

Paul, F., Arkin, Y., Giladi, A., Jaitin, D.A., Kenigsberg, E., Keren-Shaul, H., Winter, D., Lara-Astiaso, D., Gury, M., Weiner, A., et al. (2015). Transcriptional Heterogeneity and Lineage Commitment in Myeloid Progenitors. Cell *163*, 1663–1677.

Peter, I.S., and Davidson, E.H. (2011). A gene regulatory network controlling the embryonic specification of endoderm. Nature *474*, 635–639.

Pliner, H., Packer, J., McFaline-Figueroa, J., Cusanovich, D., Daza, R., Srivatsan, S., Qiu, X., Jackson, D., Minkina, A., Adey, A., et al. (2017). Chromatin accessibility dynamics of myogenesis at single cell resolution. bioRxiv. https://doi.org/10.1101/155473v1.

Qiu, X., Ding, S., and Shi, T. (2012). From understanding the development landscape of the canonical fate-switch pair to constructing a dynamic landscape for two-step neural differentiation. PLoS One *7*, e49271.

Qiu, X., Hill, A., Packer, J., Lin, D., Ma, Y.A., and Trapnell, C. (2017b). Single-cell mRNA quantification and differential analysis with census. Nat. Methods *14*, 309–315.

Qiu, X., Mao, Q., Tang, Y., Wang, L., Chawla, R., Pliner, H.A., and Trapnell, C. (2017a). Reversed graph embedding resolves complex single-cell trajectories. Nat. Methods *14*, 979–982.

Qiu, X., Zhang, Y., Yang, D., Hosseinzadeh, S., Wang, L., Yuan, R., Xu, S., Ma, Y., Replogle, J., Darmanis, S., et al. (2019). Mapping vector field of single cells. bioRxiv. https://doi.org/10.1101/696724.

Rahimzamani, A., and Kannan, S. (2016). Network inference using directed information: the deterministic limit. In 54th Annual Allerton Conference on Communication, Control, and Computing (Allerton) 2016, pp. 156–163.

Rahimzamani, A., and Kannan, S. (2017). Potential conditional mutual information: estimators and properties. In 55th Annual Allerton Conference on Communication, Control, and Computing (Allerton), (IEEE) 2017, pp. 1228–1235.

Riml, C., Amort, T., Rieder, D., Gasser, C., Lusser, A., and Micura, R. (2017). Osmium-mediated transformation of 4-thiouridine to cytidine as key to study RNA dynamics by sequencing. Angew. Chem. Int. Ed. Engl. *56*, 13479–13483.

Sanchez-Castillo, M., Blanco, D., Tienda-Luna, I.M., Carrion, M.C., and Huang, Y. (2018). A bayesian framework for the inference of gene regulatory networks from time and pseudo-time series data. Bioinformatics *34*, 964–970.

Schofield, J.A., Duffy, E.E., Kiefer, L., Sullivan, M.C., and Simon, M.D. (2018). TimeLapse-seq: adding a temporal dimension to RNA sequencing through nucleoside recoding. Time. Nat. Methods *15*, 221–225.

Schreiber, T. (2000). Measuring information transfer. Phys. Rev. Lett. *85*, 461–464.

Setty, M., Tadmor, M.D., Reich-Zeliger, S., Angel, O., Salame, T.M., Kathail, P., Choi, K., Bendall, S., Friedman, N., and Pe'er, D. (2016). Wishbone identifies bifurcating developmental trajectories from single-cell data. Nat. Biotechnol. *34*, 637–645.

Shah, S., Takei, Y., Zhou, W., Lubeck, E., Yun, J., Eng, C.-H.L., Koulena, N., Cronin, C., Karp, C., Liaw, E.J., et al. (2018). Dynamics and spatial genomics of the nascent transcriptome by intron seqFISH. Cell *174*, 363–376.e16.

Shalek, A.K., Satija, R., Shuga, J., Trombetta, J.J., Gennert, D., Lu, D., Chen, P., Gertner, R.S., Gaublomme, J.T., Yosef, N., et al. (2014). Single-cell RNA-seq reveals dynamic paracrine control of cellular variation. Nature *510*, 363–369.

Stopka, T., Amanatullah, D.F., Papetti, M., and Skoultchi, A.I. (2005). PU.1 inhibits the erythroid program by binding to GATA-1 on DNA and creating a repressive chromatin structure. EMBO J. *24*, 3712–3723.

Su, H., Wang, G., Yuan, R., Wang, J., Tang, Y., Ao, P., and Zhu, X. (2017). Decoding early myelopoiesis from dynamics of core endogenous network. Sci. China Life Sci. *60*, 627–646.

Sugihara, G., May, R., Ye, H., Hsieh, C.H., Deyle, E., Fogarty, M., and Munch, S. (2012). Detecting causality in complex ecosystems. Science *338*, 496–500.

Sulston, J., Schierenberg, E., White, J.G., and Thomson, J.N. (1983). The Embryonic Cell Lineage of the Nematode Caenorhabditis Elegans. Dev Biol. *100*, 64–119.

Sun, J., Taylor, D., and Bollt, E.M. (2015). Causal network inference by optimal causation entropy. SIAM J. Appl. Dyn. Syst. *14*, 73–106.

Svensson, V., and Vento-Tormo, R. (2017). Exponential scaling of single-cell RNA-seq in the last decade. arXiv, arXiv:1704.01379.

Swiers, G., Patient, R., and Loose, M. (2006). Genetic regulatory networks programming hematopoietic stem cells and erythroid lineage specification. Dev. Biol. *294*, 525–540.

Szklarczyk, D., Morris, J.H., Cook, H., Kuhn, M., Wyder, S., Simonovic, M., Santos, A., Doncheva, N.T., Roth, A., Bork, P., et al. (2017). The STRING database in 2017: quality-controlled protein-protein association networks, made broadly accessible. Nucleic Acids Res. *45*, D362–D368.

Takens, F. (1981). Detecting strange attractors in turbulence. Lect. Notes Math. 366–381.

Tamura, T., Kurotaki, D., and Koizumi, S.-I. (2015). Regulation of myelopoiesis by the transcription factor IRF8. Int. J. Hematol. *101*, 342–351.

Trapnell, C., Cacchiarelli, D., Grimsby, J., Pokharel, P., Li, S., Morse, M., Lennon, N.J., Livak, K.J., Mikkelsen, T.S., and Rinn, J.L. (2014). The dynamics and regulators of cell fate decisions are revealed by pseudotemporal ordering of single cells. Nat. Biotechnol. *32*, 381–386.

Treutlein, B., Brownfield, D.G., Wu, A.R., Neff, N.F., Mantalas, G.L., Espinoza, F.H., Desai, T.J., Krasnow, M.A., and Quake, S.R. (2014). Reconstructing lineage hierarchies of the distal lung epithelium using single-cell RNA-seq. Nature *509*, 371–375.

Wei, J., Hu, X., Zou, X., and Tian, T. (2017). Reverse-engineering of gene networks for regulating early blood development from single-cell measurements. BMC Med. Genomics *10*, 72.

Wiesenfahrt, T., Berg, J.Y., Osborne Nishimura, E.O., Robinson, A.G., Goszczynski, B., Lieb, J.D., and McGhee, J.D. (2016). The function and regulation of the GATA factor ELT-2 in the C. elegans endoderm. Development *143*, 483–491.

Zou, C., Denby, K.J., and Feng, J. (2009). Granger causality vs. dynamic Bayesian network inference: a comparative study. BMC Bioinformatics *10*, 122.

STAR★METHODS

KEY RESOURCES TABLE

REAGENT or RESOURCE	SOURCE	IDENTIFIER
Deposited Data		
Lung dataset	(Treutlein et al., 2014)	GEO id: GSE52583
LPS dataset	(Shalek et al., 2014)	GEO id: GSE41265
MARS-seq dataset	(Paul et al., 2015)	http://compgenomics.weizmann.ac.il/tanay/?page id=649
Olsson dataset	(Olsson et al., 2016)	synapse id syn4975060
Live imaging dataset for the *C. elegans*	(Murray et al., 2012)	Waterston lab
Software and Algorithms		
Scribe	This paper	https://github.com/aristoteleo
Rccm	Implemented based on: https://github.com/cjbayesian/rccm	https://github.com/cole-trapnell-lab/rccm
scRNASeqSim	This paper	https://github.com/cole-trapnell-lab/scRNASeqSim
Other		
Supplementary software	This paper	Supplementary software

LEAD CONTACT AND MATERIALS AVAILABILITY

Further information and requests for resources and reagents should be directed to and will be fulfilled by the Lead Contact, Cole Trapnell (coletrap@uw.edu).

This study did not generate new materials.

METHOD DETAILS

Four Possible Single-Cell Time-Series Measurement Modalities

Cell differentiation is an intrinsically noisy and asynchronous process. Even for the same developmental process, every cell in any given time should be regarded as a distinct sample. We consider four possible types of gene expression measurements in those single-cell samples:

1. Real-time, where we measure the gene expression for all the genes simultaneously in a single cell over time. This is the ideal situation but no existing technology can produce data like this yet.
2. ''RNA-velocity'' where we only capture the current state and the next state for all genes in different cells. ''RNA-velocity'' can be computationally inferred from single-cell RNA-seq datasets, or directly measured with Seq-FISH (Shah et al., 2018), and single-cell version of SLAM-seq (Erhard et al., 2019; Hendriks et al., 2018; Herzog et al., 2017; Muhar et al., 2018; Qiu et al., 2019), TUC-seq (Riml et al., 2017) and TimeLapse-seq (Schofield et al., 2018), among others.
3. Live-imaging datasets are those generated with multiple separate live-imagings for a single protein in a single-cell which are then aligned along the same developmental process to form a time-series for all genes.
4. Pseudo-time is where we apply a trajectory reconstruction algorithm to order the single-cell RNA-seq snapshot dataset to form a time-series.

The Problem of Causal Regulatory Network Inference

In this work, we formulate the problem of causal regulatory network inference as the inference of the underlying structure of influences in a stochastic dynamical system where the time series of each gene is causally regulated by a subset of other genes. We assume that there are no unobserved confounders in order to make the problem tractable. In this setting, we can potentially infer the causal regulators based on estimating the amount of information transferred from one variable (a potential regulator) to another time-delayed response variable (a potential target). In the context of single-cell genomics (e.g. scRNA-seq, live-cell imaging), we ask how we can reconstruct a regulatory network consisting of causal regulations that accurately describe the gene expression dynamics and the associated cell fate transitions.

Causal Inference

In the setting stated above, various techniques, including Granger Causality and CCM, each associated with different assumptions have been proposed to detect the structure of the causal regulatory network. In the following, we briefly summarize these methods and introduce RDI, the method we developed and used in this study.

Granger Causality

In order to determine whether one time series (X_1) is useful in forecasting another (X_2) in economics, Clive Granger first proposed Granger Causality (GC) in 1969 (Granger, 1969). According to GC, if X_1 "Granger causes" X_2, then the predictability of X_2 based on past values of X_2 and X_1 together is significantly greater than that of predicting purely based on the past values of X_2. GC in its original formulation, however, is only able to detect linear causal regulation: i.e., when the regulators regulate the target through a linear relationship.

Kernel Granger Causality

In (Marinazzo et al., 2008), a generalization of the Granger causality (kernel Granger causality or kGC) to the nonlinear case was introduced using the theory of reproducing kernel Hilbert spaces. They showed kGC outperforms linear Granger causality in the feature space of *suitable* kernel functions, assuming an arbitrary degree of nonlinearity. Hence choosing the proper kernel function with proper parameters is crucial for this method to perform acceptably. Furthermore, introducing kernel functions operating on the linear inner products means significantly higher computational complexity over that of naïve Granger causality.

Convergent Cross Mapping

In order to detect pairwise non-linear interactions in deterministic ecology systems, George Sugihara and colleagues proposed Convergent Cross Mapping (CCM) which is based on state-space reconstruction (Sugihara et al., 2012). One fundamental and somewhat counterintuitive idea of CCM, distinct from GC, is that it is possible to estimate X_1 from X_2, but not the other way if causation is from X_1 to X_2. CCM first constructs shadow manifolds M_{X_2} and M_{X_1} from lagged coordinates of the time-series X_2 and X_1. It then tests whether states in the shadow manifold M_{X_2} can be used for estimating the states in M_{X_1} and *vice versa* via mapping through nearest neighbors (*cross-mapping*). Another key idea of CCM is *convergence* which means that as the length of the time-series increases, the shadow manifolds become denser and the ellipsoid or space formed by nearest neighbors shrinks, leading to improvement of cross-map estimates. Although CCM is appealing, it cannot be generalized to stochastic systems as Takens' theorem, the cornerstone of CCM, will break down in such scenarios (Takens, 1981). Furthermore, CCM can only infer pairwise relationships and complex multifactorial interactions common in gene regulatory networks are not captured in CCM.

Restricted Directed Information (RDI)

As mentioned earlier, the causal inference method in Scribe is based on Restricted Directed Information (RDI). This measure determines the amount of *statistical inter-dependence* (or more formally the *mutual information*) between the past state of the regulator and current state of the target gene conditioned on the target's immediate previous state.

Cell state transitions are controlled by hierarchical regulatory networks (Peter and Davidson, 2011). In such networks, as the expression of the regulator changes, their downstream target responds accordingly after some time delay *d*. A canonical measure of mutual dependence which accounts for both linear and nonlinear associations between two genes (or more generally, two random variables) *X*and *Y*, is mutual information (MI) (Cover and Thomas 2006). MI is symmetric and can quantify the "amount of information" obtained about gene *X* or *Y*, through the other gene *Y* or *X*. It essentially determines how similar the joint distribution (p_{XY}) of the two genes *X*and *Y*is to the products of factored marginal distribution $p_X p_Y$, or formally:

$$I(X;Y) = \sum_{x,y} p_{XY}(x,y) \log \frac{p_{XY}(x,y)}{p_X(x)p_Y(y)}$$

If $I(X;Y)$ is zero, then the two genes *X*and *Y* are independent; otherwise it implies there exists some dependency between them (e.g. in the case of a regulator and its target). It is often useful to quantify the mutual dependence between two random variables (for example, regulator *X* and target *Y*) while removing the effect of a third random variable (for example another regulator *Z* or the history state of the target). This leads to developing of conditional mutual information, which is defined as:

$$I(X;Y|Z) = \sum_{x,y,z} p_{XYZ}(x,y,z) \log \frac{p_{XY|Z}(x,y|z)}{p_{X|Z}(x|z)p_{Y|Z}(y|z)}$$

MI provides a powerful approach to quantify the symmetric interdependence between genes. However, a favorable approach would be to measure the causal score from a potential regulator to its target. We can achieve this by considering the time-series of regulators and targets ($\underline{X}^t$, $\underline{Y}^t$) and quantifying the information transfer from the past state(s) of *X* to the current state of the variable *Y* denoted by Y_t.

Previously, T. Schreiber reported *Directed Information (DI)* as a measure for the amount of information flowing from the past state(s) of X, the regulator, to the current state of the variable Y, the target (Schreiber, 2000). DI is defined as:

$$DI(X \to Y) = \sum_{t=1}^{T} I\left(\underline{X}^{t-1}; Y_t \middle| \underline{Y}^{t-1}\right)$$

In order to remove indirect interactions, we can calculate the information transferred from the regulator to the target while conditioning on all the other genes ($\{X^{(i)}, X^{(j)}\}^C$), which is,

$$DI\left(X^{(i)} \to X^{(j)} \middle| \left\{X^{(i)}, X^{(j)}\right\}^C\right) = \sum_{t=1}^{T} I\left(\underline{X^{(i)}}^{t-1}; X_t^{(j)} \middle| \underline{X^{(j)}}^{t-1}, \left\{\underline{X^{(l)}}^{t-1}\right\}_{l \in \left\{X^{(i)}, X^{(j)}\right\}^C}\right)$$

Furthermore, for a set of genes of interest, $X^{(1)}, X^{(2)}, \ldots, X^{(N)}$ from a single-cell genomics dataset, we can infer a Directed Information graph, $G_{DI} = (V, E)$ where the vertex set V corresponds to the genes $X^{(1)}, X^{(2)}, \ldots, X^{(N)}$ and the edge $e_{ij} = (X^{(i)}, X^{(j)})$ from gene $X^{(i)}$ to $X^{(j)}$ exists if and only if $DI(X^{(i)} \to X^{(j)} \middle| \{X^{(i)}, X^{(j)}\}^C) \neq 0$ and the edge weight corresponds to the quantified DI value $DI(X^{(i)} \to X^{(j)} \middle| \{X^{(i)}, X^{(j)}\}^C)$.

It was shown that if a system is not purely deterministic, the directed information graph G_{DI} inferred from DI will correctly recover the true causal graph G_C (the network which includes all causal interactions as directed edges) (Sun et al., 2015). Although DI is able to detect both linear and non-linear causality as opposed to the linear Granger causality and is applicable to stochastic systems, it (1) can not deal with deterministic systems which may be of interest for certain scenarios and (2) poses huge computational burden because it conditions on all possible previous states of the regulator or target and (3) requires an enormous amount of data which is not affordable even with current single-cell genomic datasets.

We recently proposed a formulation of DI to alleviate those issues by employing only the immediate past of the target or regulators instead of all the past states assuming a first-order Markov system, which is generally applicable to most biological processes. In this method, the randomness is present due to the random initialization of the Markov system, hence creating a random process on which information measures are well defined. We term this method "Restricted Directed Information" (RDI) and define it as,

$$RDI_d(X \to Y) = I(X_{t-d}; Y_t | Y_{t-1})$$

Despite the fact that the original RDI measure is defined only for the immediate past of the regulator X, this measure can be flexibly defined for arbitrary effect delay d from X to Y as we have done here.

Conditional Restricted Directed Information (cRDI): Similar to (Schreiber, 2000), RDI can also be extended to the case where the information transfer from X to Y is conditioned on other potential regulator(s) Z to rule out the possible indirect causal effects and confounding factors. Thus the Conditional RDI (abbreviated as cRDI) can be formulated as:

$$RDI_{d_1}\left(X \to Y \middle| Z_{t-d_2}\right) = I\left(X_{t-d_1}; Y_t \middle| Y_{t-1}, Z_{t-d_2}\right)$$

In (Rahimzamani and Kannan, 2016), it's shown that cRDI works in many stochastic or deterministic cases and under some mild assumptions is capable of inferring the correct regulatory network G_C. Moreover, it has shown that if the conditions are violated, no other method will be able to recover the correct network (see Section IV. in (Rahimzamani and Kannan, 2016)).

In the upcoming sections we will discuss how RDI and cRDI are utilized in the Scribe toolkit.

Uniformization Method for Adjusting Sampling Bias

During our studies over the simulated benchmark data, we found that as the number of samples increases, the performance of RDI first increases and then starts to decrease. This problem was particularly acute in simulations where gene expression reached a plateau after cells committing to a cell fate. In general, while the transitional states are of higher importance in the discovery of causal interactions, oversampled equilibrium states will outnumber the transitional samples resulting in a sampling bias towards less informative equilibrium states. This phenomenon can in turn reduce the inference accuracy since RDI requires calculating conditional mutual information ($I(X_{t-d}; Y_t | Y_{t-1})$) by design, which is a function of the joint distribution ($p(x_{t-d}, y_t, y_{t-1}) = p(y_t | x_{t-d}, y_{t-1}) p(x_{t-d}, y_{t-1})$). That is, the distribution is influential in the RDI calculation, despite the fact that the RDI score should be fully determined only by the conditional distribution. Hence we devised a scheme to correct for sampling bias by re-weighting samples so that those from the system during transitional periods are weighted higher than cells sampled from the system at equilibrium. One may assume the input distribution is uniform and redistribute the observed samples in a more homogeneous fashion before calculating the RDI value.

This bias correction scheme, which we term *Uniformized conditional mutual information* (uCMI) replaces the actual distribution $p(x_{t-d}, y_{t-1})$ with a uniform distribution $u(x_{t-d}, y_{t-1})$ and then calculates the conditional mutual information for $p(y_t | x_{t-d}, y_{t-1}) u(x_{t-d}, y_{t-1})$. This is made possible thanks to the concept of *potential Conditional Mutual Information* (qCMI) (Rahimzamani and Kannan, 2017) and an estimator, in which the actual distribution $p(x_{t-d}, y_{t-1})$ of samples is replaced by any arbitrary distribution

$q(x_{t-d}, y_{t-1})$ before estimating the conditional mutual information. uCMI is thus a special case of qCMI, in which the replacement distribution $q(x_{t-d}, y_{t-1})$ is uniform. By replacing the conditional mutual information (CMI) in RDI with uCMI, we obtain a new way of computing information transfer called *uniformized Restricted Directed Information* (uRDI).

The discussion above is especially relevant for single-cell genomics datasets as single cells are not homogeneously spread across many biological processes and they often will be heavily sampled from steady states while rarely from transition states. A compelling discussion of this phenomenon can be found in c.f. (Olsson et al., 2016). This imbalance of sampling confounds the performance of RDI (or other mutual information based methods) and thus leads to ignorance of rare but critical regulation that happened during transition states. We noticed that empirical methods have been reported to account for sampling biases from single-cell measures (Krishnaswamy et al., 2014). However, the uRDI method incorporated in Scribe provides a rigorous approach to replace the biased sampling distribution with a uniform distribution to quantify potential causality (how much influence a regulator can potentially exert on target without cognizance of the regulator's distribution) and is thus arguably a superior approach to account for the sampling biases issue (Rahimzamani and Kannan, 2017).

Scribe: A Toolkit for Visualization and Detection of Complex Causal Regulation from Single-Cell Genomics Datasets

Although Scribe is applicable to any time-series datasets, it is specifically designed for visualizing and detecting complex gene regulation from single-cell genomics datasets (e.g. scRNA-seq). Scribe relies on (uniformized) restricted directed information to detect causality but also supports other methods, including the well-known mutual information, Granger causality and the more recent CCM. Scribe starts with time-series data, which can be based on "pseudotime-series" of a developmental trajectory reconstructed from scRNA-seq data such as those constructed using Monocle 2, live imaging data or datasets with current and predicted spliced RNA expression estimated using RNA-velocity. Scribe provides two main types of analysis:

1. Visualization and estimation of causal gene regulation;
2. Reconstruction of large-scale sparse causal regulatory networks.

Preparing Pseudotime-Series or RNA-Velocity for scRNA-seq Datasets

Scribe does not provide any built-in functionalities for pseudotime-series construction and relies on Monocle (http://cole-trapnell-lab.github.io/monocle-release/) or similar tools, such as dpt (Haghverdi et al., 2016) or wishbone(Setty et al., 2016), for reconstructing the single-cell trajectory before inferring causal networks. Scribe also doesn't provide any built-in functionalities for RNA-velocity estimation and relies on the velocyto framework (La Manno et al., 2018) for those estimations. In relation to physical time, pseudotime has an arbitrary scale, thus Scribe doesn't consider pseudotime value themselves instead using the ordering of each cell in pseudotime for causal network inference. Similarly, we also assume the time delays Δt used in RNA-velocity estimations are constant across cells and genes for the sake of simplicity.

Visualizing Pairwise Gene Interaction

In order to intuitively visualize casual regulations between genes, Scribe provides different strategies to visualize the response, causality and combinatorial **regulatory logic between gene pairs**. The response visualization is similar to the DREVI approach as proposed by Smita Krishnaswamy, et. Al (Krishnaswamy et al., 2014) with the exception that it considers time delay to visualize the expected expression of potential targets given a potential regulator's expression after a time delay. Response visualization thus additionally aids in visualizing commonly appeared time-delayed regulations involved in cell differentiation (Alon, 2007).

One limitation of response visualization is that it ignores the effects of a gene's previous state to the current state or memory of its history. In order to also capture this effect and thus intuitively visualize causality, Scribe is equipped with causality visualization. Essentially, this approach visualizes the causal regulation by considering the information transfer from the time-delayed potential regulator to the target's current expression, conditioned on the target's previous state to remove effects from auto-regulation. Causality visualization is a heatmap consisting of the expected value of the target's current expression given the target's immediate past expression (y-axis) and the regulator's expression with a time lag *d* (x-axis). For each column, it represents the relationship for the target's expression at the previous time point to the current state (memory of the history or "auto-regulation") given a fixed regulator value, while for each row, the information transfer from the regulator to its targets given the previous target state.

Visualizing Combinatorial Gene Regulation

It is of great interest to understand the combinatorial gene regulation as it often determines how cells make decisions to choose a particular cell fate or adapt to external stimuli (Ma et al., 2009). In order to visualize two-input combinatorial regulation, Scribe provides a third visualization tool. This visualization is a heatmap consisting of the expected value of the target's current expression given knowledge of both of the regulators' expressions with a time lag (x/y-axis). For both of the causality and the combinatorial logic visualizations, the corresponding expected value is calculated through a local average with a Gaussian kernel.

We noticed that gene regulation *directly* affects the rate of the target gene which then results in gene expression changes. For example, if a gene X is negatively regulated by gene Y. We may define the rate function of X as $\frac{dX_t}{dt} = 1/(X_{t-1}^2 + Y_{t-\mu}^2)$. Therefore, visualizing the expected rate of a target at its current state given knowledge of both the regulators' expressions with a time lag (x/y-axis) allows better intuition of regulations. Although we won't have accurate estimates of the rate of gene expression with pseudo-time series data, the RNA-velocity method can be used to obtain those estimates.

Causal Network Inference: an RDI-Based Algorithm

Causal inference in Scribe is based on RDI, which is an extension of directed information under the assumption that the underlying processes can be described by a first-order Markov model. The method we implemented basically tries to calculate the RDI value for each pair of genes (*i*,*j*) conditioned over the top *L* genes (default is 0 or no conditioning and 1 for cases where we used conditioning) which are candidates of being regulators of the gene *j*.

To reach this goal, it first calculates all the pairwise *unconditioned* RDI values, for all the potential delays specified by the user in vector *d* (by default, it is a vector including 5, 10, 20, 25). Note that for the RNA-velocity dataset, since we assume the time delays Δt for the current and predicted future RNA expression level are constant across the cell and genes, there is no need to scan for a window of potential time delays. Then for each pair (*i*, *j*), it treats the delay corresponding to the largest RDI value as the "*true*" *delay of effect*, i.e. the actual time delay by which the effect of *i* appears in *j*. Having identified the "true" delays, the method then re-calculates the pairwise RDI values for each pair of genes (*i*, *j*), this time conditioned over the top *L* (*L*can be specified by the user) genes with the highest incoming RDI values to *j* associated with their corresponding true delays, treating them as the potential regulators of *j*.

The algorithm of causal inference in Scribe is as follows:

Input: Gene Expression Time-Series (Either Based on Pseudotime-Series, "RNA-velocity" or Live Imaging Data, among Others) $\underline{X^{(i)}}^{t}$ for Each Gene *i*
Output: A Matrix of Pairwise Causality Scores
Parameters: *d*: Vector of Delays, *L*: Number of Conditioning Genes
Pseudocode:

```
1. For each pair of genes (i, j):
   - For all delays $\delta \in d$: Calculate $RDI_\delta(X^{(i)} \rightarrow X^{(j)})$
   - Set $\delta_{i,j}^{\max} := \underset{\delta \in d}{\mathrm{argmax}} RDI_\delta(X^{(i)} \rightarrow X^{(j)})$
2. For Each Gene j:
   - for All i: Sort $RDI_{\delta_{i,j}^{\max}}(X^{(i)} \rightarrow X^{(j)})$ Values in Descending Order
   - According to the Sorting above, Take the $L+1$ Nodes i with the Highest Incoming RDI Values to j and Store Them in a Set
     as $inc_j^{\max}$. Store Their Corresponding Delays $\delta_{i,j}^{\max}$ in a Set $d_j^{\max}$.
3. for Each Pair of Genes $(i,j)$:
   - If $i \in inc_j^{\max}$, Remove i from $inc_j^{\max}$. Otherwise, Remove the Node l with the Lowest $RDI_{\delta_{l,j}^{\max}}(X^{(l)} \rightarrow X^{(j)})$ from $inc_j^{\max}$.
4. for Each Pair of Genes $(i,j)$: Output $RDI_{\delta_{i,j}^{\max}}(X^{(i)} \rightarrow X^{(j)} \,|\, \{X_{t-\delta_{l,j}^{\max}}^{(l)}\}_{l \in inc_j^{\max}})$
```

To calculate the causal network with uRDI, we apply the same algorithm as above but simply replace RDI with uRDI. In addition to what required in RDI, uRDI also needs to estimate the actual distribution, $p(x_{t-d}, y_{t-1})$, which relies on kernel density estimation (KDE). We use standard Gaussian kernels from R in the Scribe package to calculate KDE.

Inferring and Visualizing Transcriptomic Gene Regulatory Network

Scribe can estimate a causal network from a set of known TFs (and among the TFs) to a set of targets of interest (selected through, for example the BEAM test) , or estimate the pairwise causality among all the genes in a set of genes of interest. For the first scenario, Scribe estimates causality between all pairs of TFs and the causality from each TF to each putative target; for the second scenario, Scribe estimates causality for any pair of genes in both directions. In order to retrieve significant causal edges while removing promiscuous edges and reconstruct a sparse causal regulatory network that satisfies known properties of biology networks, Scribe relies on a modified CLR regularization method (*Context Likelihood of Relatedness*) regularization and a directed network regularization inspired by some biological assumptions (see section ***Network sparsifier: CLR regularization and directed graph regularization*** below).

In order to facilitate the visualization of complex networks, Scribe provides a variety of approaches to visualize the RDI network either through a heatmap, a hierarchical layout, an arc diagram or a hive plot, implemented based on *igraph*, *netbiov*, *ggraph*, *arcdiagram* as well as the *HiveR* R packages.

We used the Kleinberg centrality to define the hubness used to order genes on the arc plot which is defined as the principal eigenvector of AA', where A is the adjacency matrix of the graph (Kleinberg, 1999).

In addition to the core causality detection feature based on (uniformized) restricted direction information, Scribe also supports various methods for inferring the regulatory relationships including mutual information, Granger causality, and CCM implemented based on *parmigene*, *vars*, and the *rEDM* packages, respectively. We also provide a python package for most of the estimation methods, although without extensive support for visualization which may be supported in the future.

Parameters of RDI

The estimation of mutual information is inspired by Kraskov's method (Kraskov et al., 2004) which builds on counting nearest-neighbor points. In the R implementation of Scribe, nearest-neighbor points are identified with a modified RANN package.

Parameter	Type	Effect of Tuning Parameters
d	**Vector of positive integers**	Default: 5, 20, 40 The vector of potential delays, for which the corresponding RDI values are calculated. Setting this argument too small may limit the ability of Scribe to detect causal relationships, while setting it too large can result in the discovery of incorrect or indirect causal relationships, resulting in false delays and conditioning.
L	**Non-negative Integer**	Default: 0 The number of the top incoming node(s) to the target, excluding the source, over which RDI is conditioned. $L = 0$ corresponds to no conditioning (Plain pair-wise RDI). Any $L>0$ corresponds to conditional RDI (cRDI). Conditioning over more nodes approaches the theoretical prerequisite of conditioning over all genes, excluding the source and target, needed for inferring the true causal network, however it imposes more computational burden and undesirably reduces the accuracy of the RDI estimator with fixed number of samples N, as it exponentially increases the dimension of the state space used to calculate the k-nearest neighbors.
k	**Positive Integer**	Default: 5 Number of the nearest neighbors in the kNN estimator for the conditional mutual information. The parameter should be set in such a way so the neighborhood captures an adequate number of samples for a good estimate of the probability corresponding to each sample.
Uniformization	**Boolean**	Default: False If True, uRDI instead of RDI will be used. While imposing higher computational burden over the same data than RDI, uRDI is expected to improve the causal inference in the cases with highly-biased sampling distributions.

Algorithm Complexity

Algorithm	Methodology	Parameters	Worst-Case Complexity *N*: the Number of Samples; *d*: the Dimension of the *X* and *Y* Manifolds (Default 2); *k*: the Number of Nearest Neighbors *L*: the Number of Conditioning Genes *l*: the Dimension of the Features Data
CCM	Determining the causality from *X* to *Y* based on how well one can reconstruct the cross-mapped estimate of *X* from the nearest neighbors determined on *Y* space	*E*: The number of lags embedded in the shadow manifold **Tau**: The time lag between each consecutive pair of time samples (default: 1)	$O(2EN \log N)^{*}+O(2(E+1)N)^{**}$ *Complexity of kd-tree algorithm for kNN search ** Complexity of regression and weight estimation
Granger Causality	Determining the causality from *X* to *Y* based on how much the past samples of *X* contribute in linearly estimating the current state of *Y*, compared to when the *Y* is estimated based merely upon its own past	**Maxlag**: The number of lags of the past sample included in estimating the current state of *Y*	$O(lN+2l^2N+l^3)^{*}$ * The complexity of linear regression
RDI and cRDI	Determining the causality from *X* to *Y* based on the amount of mutual information between the past of *X* and the current state of *Y* conditioned over the past of (potentially) all other variables than *X*	*k*: The number of neighbors for kNN estimation of mutual information *d*: The lags for which the mutual information from the lagged source to the current state of target is estimated. *L*: The number of the conditioning nodes other than *X* and *Y*. While small *L*'s can result in false positives since we won't filter out confounding and/or intermediate factors, too large *L*'s will result in curse of dimensionality in smaller sample set regimes and increasing the computational complexity in larger sample set regimes.	$O((d+L+1)N \log N)^{*}+O(kN)^{**}$ *Complexity of kd-tree algorithm **Complexity of inquiry of each neighbor
uRDI and ucRDI	Same as RDI method, but including the replacement of the empirical distribution of the past samples with a uniform distribution	**All Parameters from RDI plus:** **BW**: The bandwidth of the kernel estimator	$O((d+L+1)N \log N)^{*}+O(kN)^{**}+O(N^3)^{***}$ *Complexity of kd-tree algorithm **Complexity of inquiry of each neighbor ***Complexity of kernel density estimation

Regularizing Causal Interaction Networks

In theory, Scribe can remove potential indirect causal gene regulation from one gene *X* to another gene *Y* by conditioning on all other genes in the transcriptome except *X*. However, this requires a huge number of samples which is infeasible even with current single cell genomics techniques and is impractically slow for even modest sets of genes. Therefore, we sought alternative approaches based on statistical significance and reasonable assumptions of biology structures to remove potential indirect edges. The first method we applied is the CLR or *Context Likelihood Relatedness* regularization. Previously, CLR is used in conjunction with mutual information (MI). RDI (cRDI, etc) is like MI, it calculates the pairwise "causality influence score". Simply computing MI between all pairs of genes would yield a dense network with many indirect interactions. CLR regularizes this network to enrich it for direct interactions. Just as with MI, we need some means of sparsifying the network formed by RDI links between all pairs of genes. Thus, Scribe uses a procedure for regularizing RDI networks that is analogous to the one CLR uses to regularize MI networks. It works as the following: after computing the causality score with RDI (uRDI) without conditioning between all gene-pairs, CLR calculates a normalized score based on the z-score (or 0 if the z-score is less than 0) from all the input edges to the potential target and all the output edges from the potential regulator of the gene pair. This normalized score is used as a statistical likelihood of each causal edge regarding to its network context. More formally, denoting the asymmetric matrix R corresponds to all raw causality scores calculated with Scribe, with R_{ij} being the causality score from gene i to gene j, we can calculate the z-score z_i based on all gene i's output causality scores and z_i all gene j's input causality scores. The normalized score of R_{ij}, $\widehat{R}_{ij}$ is defined as:

$$\widehat{R}_{ij} = \sqrt{\max(0,z_i)^2 + \max(0,z_j)^2} \Big/ 2$$

The user can either use the normalized score or choose a threshold of the normalized scores and treat the edges above the threshold as significant or real regulation comparing to the background distribution of the causality scores. As discussed in the original study, CLR removes many of the false regulations in the network by eliminating "promiscuous" cases, where one regulator weakly co-varies with a large numbers of genes, or one gene weakly co-varies with many transcription factors which may arise when the assayed conditions are inadequately or unevenly sampled. We note that, however, the original CLR is only applied on a symmetric mutual information based matrix while we are dealing with an asymmetric matrix of causality scores. To avoid potential confusion, we name our modified procedure as "CLR regularization" in our text. After applying CLR, the network may be still dense and contain spurious edges. Previous studies have shown that the biological networks have some special properties distinct from those of random networks; for example, the network's out-degree distribution is well approximated by a power law distribution where its in-degree distribution is almost an exponential distribution. Based on those assumptions, we proposed a new regularization method for a directed graph.

The goal of our method is to learn a sparse directed graph from a dense asymmetric causality network (retrieved after applying CLR regularization) satisfying two aforementioned properties. The directed graph's structure is represented by an indicator matrix denoted by $\Theta \in \{0,1\}^{N\times N}$, where $\theta_{i,j} = 1$ stands for the existence of edge i to j, and 0 otherwise. Since the entries are indicators, the in-degree and out-degree of each node in the network can be easily formulated. Specifically, the out-degree of the ith node can be represented by $h_{out}(i) = \|\theta_i\|_1$ and the in-degree of the ith gene is correspondingly represented by $h_{in}(i) = \|\theta^i\|_1$, where θ_i and θ^i are the ith row and ith column of Θ, and ℓ_1-norm counts the number of nonzero elements since $\theta_{i,j} \in \{0,1\}$. Given the asymmetric matrix of causality score R with the (i,j)-th entry as R_{ij}, the following optimization problem is formulated to learn the structure of the network:

$$\min_{\Theta \in \mathcal{A}} \left(-\sum_{i,j} \theta_{i,j} R_{i,j} + \alpha \sum_{i=1}^{N} \log(\|\theta_i\|_1 + \xi) + \lambda \sum_{i=1}^{N} \|\theta^i\|_1 \right)$$

where the feasible set of the network structure is

$$\mathcal{A} = \left\{ \Theta \in \{0,1\}^{N\times N} : \sum_i \sum_j \theta_{i,j} \geq B \right\}$$

The intuition of the objective function comes directly from the above three assumptions: the first term of the objective is to select the edge with large value of R_{ij}; the second term is the negative log likelihood of the power law distribution for the out-degree of each gene; the last term is the negative log likelihood of the exponential distribution for the in-degree of each gene. The budget parameter B is introduced to prevent trivial solution, and a small positive value ξ is used to prevent the numerical issue of log function. The parameter α is the exponent of the power law distribution and λ is the parameter of the exponential distribution.

Benchmarking Scribe with Alternative Algorithms on Inferring Causal Regulatory Network

We follow the same procedure as reported previously (Qiu et al., 2012) to simulate the differentiation of central nervous system (Equation 1), except here we replace the correlated noise in the previous study with independent additive noise for the purpose of simplicity. The data generated through this simulation is regarded as "real-time" dataset.

$$mature_{\mu} = 0$$

$$n = 4$$

$$k = 1$$

$$a = 4$$

$$\eta = .25$$

$$\eta_m = 0.125$$

$$\eta_b = 0.1$$

$$a_s = 2.2$$

$$a_e = 2.2$$

$$m_x = 10$$

$$\begin{aligned}
\frac{dx[Pax6]}{dt} &= a_s \frac{1}{1 + \eta^n \left(x_{t-1}[Tuj1] + x_{t-1}[Aldh1L] + x^n_{t-1}[Olig2]\right) x^n_{t-1}[Mature]} - k \bullet x_{t-1}[Pax6] \\
\frac{dx[Mash1]}{dt} &= a \frac{x^n_{t-1}[Pax6]}{1 + x^n_{t-1}[Pax6] + x^n_{t-1}[Hes5]} - k \bullet x_{t-1}[Mash1] \\
\frac{dx[Brn2]}{dt} &= a \frac{x^n_{t-1}[Mash1]}{1 + x^n_{t-1}[Mash1]} - k \bullet x_{t-1}[Brn2] \\
\frac{dx[Zic1]}{dt} &= a \frac{x^n_{t-1}[Mash1]}{1 + x^n_{t-1}[Mash1]} - k \bullet x_{t-1}[Zic1] \\
\frac{dx[Tuj1]}{dt} &= a_e \frac{x^n_{t-1}[Brn2] + x^n_{t-1}[Zic1] + x^n_{t-1}[Myt1L]}{1 + x^n_{t-1}[Brn2] + x^n_{t-1}[Zic1] + x^n_{t-1}[Myt1L]} - k \bullet x_{t-1}[Tuj1] \\
\frac{dx[Hes5]}{dt} &= a \frac{x^n_{t-1}[Pax6]}{1 + x^n_{t-1}[Pax6] + x^n_{t-1}[Mash1]} - k \bullet x_{t-1}[Hes5] \\
\frac{dx[Scl]}{dt} &= a_e \frac{\eta^n x^n_{t-1}[Hes5]}{1 + \eta^n x^n_{t-1}[Hes5] + x^n_{t-1}[Olig2]} - k \bullet x_{t-1}[Scl] \\
\frac{dx[Olig2]}{dt} &= a_e \frac{\eta^n x^n_{t-1}[Hes5]}{1 + \eta^n x^n_{t-1}[Hes5] + x^n_{t-1}[Scl]} - k \bullet x_{t-1}[Olig2] \\
\frac{dx[Stat3]}{dt} &= a \frac{\eta^n x^n_{t-1}[Hes5] x^n_{t-1}[Scl]}{1 + \eta^n x^n_{t-1}[Hes5] x^n_{t-1}[Scl]} - k \bullet x_{t-1}[Stat3] \\
\frac{dx[Myt1L]}{dt} &= a \frac{x^n_{t-1}[Olig2]}{1 + x^n_{t-1}[Olig2]} - k \bullet x_{t-1}[Myt1L] \\
\frac{dx[Aldh1L]}{dt} &= a_e \frac{x^n_{t-1}[Stat3]}{1 + x^n_{t-1}[Stat3]} - k \bullet x_{t-1}[Aldh1L] \\
\frac{dx[Sox8]}{dt} &= a \frac{\eta^n_m x^n_{t-1}[Olig2]}{1 + \eta^n_m x^n_{t-1}[Olig2]} - k \bullet x_{t-1}[Sox8] \\
\frac{dx[Mature]}{dt} &= mature_{\mu} \left(1 - \frac{x_{t-1}[Mature]}{m_x}\right)
\end{aligned} \tag*{Equation 1}$$

Ordinary Differential Equations for the Neuron System

For creating Figures S1B and S1D, we set the time step as 0.1, samples per simulation as 100, the total number of simulations as 20. We then infer the causal network based on all the 2000 samples using CCM, GC and RDI or uRDI either without conditioning or conditioning on one gene that has the maximal input causality other than the current regulator to the target. Time delay between regulator and target used in all those algorithms is set to be 1. We compare the inferred network with the known network to calculate the AUC (area under curve). The experiment is repeated for 25 times to ensure reliable conclusions. We also increase the standard deviation of the intrinsic noise from 0 to 0.2. ROC (Receiver Operating Characteristic) curve in Figures S1C and S1D is obtained similarly while setting the simulation based on a linear system where the transition matrix A is generated according to the network with non-zero coefficients randomly taken from a uniform distribution $u(0.75,1.25)$. The A matrix is then normalized to $1.01 \times \max\{eig(A)\}$ to avoid the divergence of the system. The intrinsic noise standard deviation (s.d) is set to be equal to 0.01. All the genes are initialized with a random value $u(0.5,2)$. To infer the causal network, we take 100 samples per simulation and perform the simulation five times, then apply Scribe, CCM and GC on those simulated data points.

To visualize the response, causality and combinatorial regulations as in Figures S2C–S2I, a single simulation leading to the neuron fate is used. To create the response and the causality visualization for the two-node motifs (Ma et al., 2009), the network motifs are firstly converted into a set of SDE functions using similar formulations as that used in the above simulation for neuronal differentiation. The expression dynamics is then simulated by setting the initial expression for both genes as 0.01 and followed based on the set of SDE equations (Figure S2A). We used similar procedures to simulate expression of genes under combinatorial regulations with different logic gates and then create the combinatorial regulation visualizations (Figure S2B).

To investigate the importance of temporal coupling and the number of samples on the performance of causal inference, we also simulate three other types of dataset based on the simulated "real time" dataset as following:

1. The RNA-velocity analysis framework estimates both exon and intron expression levels for each cell i or C_i. It then calculates the RNA-velocity $V^i(j)$ for each gene j in each cell i and predicts the future exon expression of $E^{predict}$ after $\Delta t = 1$. Assuming the time delays from all regulators to their putative targets are the same as Δt (or 1), Scribe calculates causality from the potential regulator to the target with the conditional mutual information between the current regulator's exon expression X_t to the predicted target exon expression Y_{t+1} (or equivalently the estimated RNA velocity value $V_t(Y)$) conditioned on the current target exon expression Y_t or by the default formula $I(X_t;Y_{t+1}|Y_t)$ (or alternatively $I(X_t;V_t(Y)|Y_t)$). Since X_t, $Y_{t+1}(V_t(Y))$ and Y_t are all estimated from the same cell, in theory the gene expression dynamics between X_t, $Y_{t+1}(V_t(Y))$ and Y_t is coupled. To generate RNA-velocity simulation dataset, we randomly select one time point t for each cell and collect all genes' current and the next time point's expression ($X_t^{(i)}$ and $X_{t+1}^{(i)}$). RNA velocity for each cell in that time point is then simply calculated as the difference between next time point and current time point's gene expression ($V_t(X^{(i)}) = X_{t+1}^{(i)} - X_t^{(i)}$).
2. To generate live-imaging simulation dataset, we first randomly select 13 cells where for each cell, a different gene is chosen and is followed over the entire developmental process.
3. To generate pseudotime dataset, similar to RNA-velocity, we randomly select one time point t for each cell and collect all genes' expression at that time point. Then all data points from each cell at different time point is pooled and used as input to Monocle 2 for trajectory inference, we then set the beginning of the simulation as root state for the trajectory and order cells based on the inferred pseudotime to form a pseudotime series.

To create Figure S4B, five replicates each with 2000 data points are used for each algorithm. For Figures S4C and S4D, the same analysis is performed but with data (replicates) downsampled to 200, 400, 600, 800, 1000, 1200, 1400, 1600, 1800 or 2000 data points (1, 5, 10, 15, 20 repeats).

Details on Analyzing Datasets Used in This Study

Benchmark Scribe with DREAM Challenge Datasets

In GeneNetWeaver, we looked at the DREAM3 challenge in-silico data for three networks, each of which has a size of 50. All networks were obtained from modeling network in yeast (Yeast-1, Yeast-2 or Yeast-3). For each network, GeneNewWeaver is used to simulate the time series for 10 times (i.e. we had a total of 10 runs), for a duration of 1000 time-units, and the measurement is recorded at every 10 time-units, hence 100 total time points for each run. The intrinsic noise coefficient was set to be 0.05. The measurement noise was set as the default model in microarrays which is also used in DREAM4 challenge. Each time series was then normalized after adding the noise. For each of the three networks, we conducted the inference task by running different methods over the generated time series data described above and compared the final AUC score for each network.

Inferring Causal Network with Pseudotime Ordered scRNA-seq Datasets

Lung data is processed as described previously. Expression matrix is downloaded from GEO (GSE52583). After filtering, log-transformed TPM values of 183 single cells' transcriptome are used for monocle 2 analysis. (Qiu et al., 2017a). Categorization of pneumocyte specification markers into either early and late groups used for benchmarking is based on references (Qiu et al., 2017a; Treutlein et al., 2014).

The LPS data was pre-processed as described previously. 510 cells annotated as unstimulated replicate (normal unstimulated cells were observed to have low RNA library quality), LPS stimulated cells without any perturbations, and LPS stimulated cells with Stat1 and Ifnar1 knocked out taken at each of the included time points are used. The pseudotime trajectory is reconstructed with the reversed graph embedding (Qiu et al., 2017a) on the same set of ordering genes used in this study. Only the path with wild-type cells is used for causal network inference. Regulators and targets, and the regulatory network used for benchmarking are collected from references (Amit et al., 2009) and reference (Garber et al., 2012), respectively.

Olsson data is processed as described previously. The processed FPKM values is downloaded via synapse (id syn4975060) and used for pseudotime ordering with Monocle 2. The master regulators, transcription factors and downstream targets, and the regulatory network used for benchmarking are collected from reference (Qiu et al., 2017a) and references (Su et al., 2017), respectively.

Paul data is processed as described previously. We downloaded the UMI counts data and the cell cluster annotation information for the Paul from http://compgenomics.weizmann.ac.il/tanay/?page id=649. Only the path leading to the erythrocytic fate is used for reconstructing the causal regulatory network. The regulatory network responsible for the differentiation of erythrocyte cells used for benchmarking is collected from (Swiers et al., 2006).

Infer Causal Network with RNA-Velocity

The data of the chromaffin cell "RNA-velocity" analysis is retrieved from (http://pklab.med.harvard.edu/velocyto/notebooks/R/chromaffin.nb.html). We use the estimated exon expression to reconstruct the trajectory for the chromaffin cell commitment. Only cells on the path from the Schwann cell progenitors to mature chromaffin cells are used to infer the casual network. Two different formulations, $I\ (X_t;\ Y_{t+1} \mid Y_t)$ (or $I\ (X_t;\ V_t\ (Y) \mid Y_t)$), can be used to infer causal networks with data from RNA-velocity. In this study, we apply the first formulation.

Inferring Causal Network with Live-Image Data

Lineage-resolved live-imaging data for *C. elegans* early embryogenesis is obtained from Waterston lab. Raw fluorescence intensity signal is directly used for causal network inference. We note two caveats in analyzing the reporter data with Scribe. First, although the promoter-fusion data sheds light on the induction kinetics of the TF of interest, once the fluorescent reporter is expressed it follows the trafficking and degradation kinetics of the histone protein, and not the TF. Second, the time series for each TF was captured in a different embryo, so this may introduce noise that obscures the regulator/target relationships between the TFs although the *C. elegans* development process is highly robust. Nevertheless, this data set represents an unprecedented view of TF activity at high spatiotemporal resolution during the early development of a complex organism.

DATA AND CODE AVAILABILITY

Code Availability

A version of Scribe (version: 0.99) used in this study is provided as Supplementary Software. The newest Scribe implemented as an R package is available through GitHub (https://github.com/cole-trapnell-lab/Scribe), an equivalent python version is hosted at (https://github.com/aristoteleo/Scribe-py). Notebooks for usage cases of Scribe is available at https://github.com/aristoteleo/Scribe-Python-notebooks. CCM algorithm is implemented as the rccm package (https://github.com/cole-trapnell-lab/rccm) which is based on https://github.com/cjbayesian/rccm. The neurogenesis simulation is implemented as the scRNASeqSim package (https://github.com/cole-trapnell-lab/scRNASeqSim). Supplementary Software also includes a helper package containing helper functions as well as all analysis code that can be used to reproduce all figures and data in this study.

Data Availability

This study did not generate new data.